Measurement Science and Technology

Miniaturized interferometric confocal distance sensor for surface profiling with data rates at ultrasonic frequencies

OPEN ACCESS
IOP Publishing
Measurement Science and Technology
Meas. Sci. Technol. **34** (2023) 045104 (9pp)
https://doi.org/10.1088/1361-6501/acaf97

Miniaturized interferometric confocal distance sensor for surface profiling with data rates at ultrasonic frequencies

Sebastian Hagemeier[1,*], Kai Bittner[2], Frank Depiereux[2] and Peter Lehmann[1]

[1] Measurement Technology Group, Faculty of Electrical Engineering and Computer Science, University of Kassel, Wilhelmshoeher Allee 71, Kassel 34121, Germany
[2] Fionec GmbH, Ritterstraße 12a, 52072 Aachen, Germany

E-mail: sebastian.hagemeier@uni-kassel.de

Received 16 September 2022, revised 21 December 2022
Accepted for publication 3 January 2023
Published 12 January 2023

Abstract

Point-wise measuring profilometers like the tactile stylus instruments or optical sensors are established measurement tools in science and industry to measure and characterize surface textures. We present a fiber-coupled laser interferometric confocal distance sensor for surface profiling. The sensor is characterized by small geometric dimensions and by its high lateral scanning speed. The ability to measure specularly reflecting and rough surface textures are demonstrated by performing several measurements on a sinusoidal standard as well as two roughness standards specified by different degree of roughness using various lateral scan velocities up to 75 mm s^{-1}. These measurement results are compared to those obtained by a tactile stylus instrument used in the identical measurement environment as the introduced optical sensor. Finally, the ability for full-field measurements is presented.

Keywords: high-speed sensor, interferometric confocal distance sensor, optical profilometer, miniaturized point sensor, fiber coupled sensor, roughness measurement, fiber optics

(Some figures may appear in colour only in the online journal)

1. Introduction

Optical point sensors are often combined with mechanical scan axes to measure surface profiles or topographies in industry and science. Due to a higher lateral scan velocity and a contactless measurement, these optical sensors provide an alternative to tactile stylus instruments. Fundamental advantages against often used optical full-field measuring topography sensors are a more compact geometrical setup, a high lateral scan range and a flexible sensor probe, enabling measurements at hard-to-access surface structures of the object under investigation [1–4]. A disadvantage compared to full-field measuring sensors is that lateral scan axes are necessary to achieve the full surface topography to be measured by stitching single height values. In order to reduce the number of mechanical scan axes several approaches exist [5, 6].

Optical point-wise measuring sensors are available on the basis of various physical operating principles. One example is given by the chromatic confocal sensor where the axial depth discrimination is performed by wavelength dependent focus lengths of an objective lens [7–9]. Hence, no mechanical scan axis is necessary for the depth scan. However, to achieve a good optical performance (e.g. limited chromatic aberrations) due to the necessary broadband light source, microscope objective lenses are commonly used, which limits the geometrical dimensions of the sensor. Furthermore, the axial scan range is limited by the range spanned by the wavelength dependent focal lengths. An extension can be achieved using diffractive optical elements [10, 11], which leads to additional

* Author to whom any correspondence should be addressed.

technological effort. Another point-wise measuring sensor is a laser focus sensor (LFS) where the measurement principle is based on astigmatism or Foucault knife-edge method. Mastylo *et al* [12] present an LFS with an axial measuring uncertainty in a range of 0.7 nm to 2 nm and a lateral scan velocity limited by 6 mm s^{-1}. Further sensors use interferometric working principles. A fiber-coupled coherence scanning interferometer without mechanical scan axis to perform the depth scan is shown in [13–15]. Here, the depth scan is achieved by a tilted reference mirror. A further benefit of this sensor is provided by a fiber-end acting as probe head and thus, exhibits flexible geometrical dimensions to reach even hard-to-access measurement areas. However, a line scan camera is used to detect an interference signal related to one single height value. As a consequence, the acquisition rate is limited by the scan rate of the camera. Moreover, due to the intensity offset, the contrast of an interference signal is limited by the dynamic range of the camera. In [16, 17] a Fizeau interferometer is presented where the optical path length difference (OPD) is sinusoidally modulated using a bending beam to generate an oscillating motion of the probe head in axial direction. Due to the mass inertia of the probe head, the used oscillation frequencies are usually limited to values below 1 kHz. Since the maximum acquisition rate of height values corresponds to twice the oscillation frequency, the measurement data rate is limited to below 2 kHz. The usage of higher oscillation frequencies is also possible, as discussed in [16]. A similar approach of a common-path interferometer is introduced by Sharma *et al* [18, 19], where the sinusoidal modulation of the OPD is achieved either by stretching the fiber-end of the probe head using a piezoelectric transducer or by an electro-optical phase modulation using an $LiNbO_2$ crystal. While the oscillation frequency and also the measurement data rate are limited to 1.25 kHz in case of the piezoelectric transducer, these values increase up to 5 kHz for the electro-optical modulator.

In this contribution, we present a miniaturized interferometric-confocal distance sensor (ICDS) providing a measurement data rate up to 80 kHz, which is an extended version of the sensor shown in [20]. After presenting the sensor setup and its working principle, the sensor's performance is validated by measurements on different surface textures. Besides the ability to measure on specular surfaces, it is shown that the sensor is able to measure rough surface textures and to determine roughness parameters, which is often a required ability in industrial applications.

2. Working principle

In this section, first the miniaturized interferometric sensor setup is introduced. Then, the signal characteristics and analysis of interference signals obtained with the fiber-coupled interferometric distance sensor with oscillating reference mirror are explained.

2.1. Sensor setup

The working principle of the point-wise measuring ICDS is related to a Linnik interferometer setup [21]. Laser light is used for illumination and transferred via a single-mode fiber to the interferometric setup shown in figure 1(a). The light transmitting through the fiber end face is collimated by a gradient index lens and separated into a measurement and a reference arm by a beam splitter cube. The portions of light are focused on the surface of the specimen and the reference mirror, respectively, using an aspherical focusing lenses. The light reflected from the specimen and the reference mirror is collected by the corresponding lens, superimposed by the beam splitter cube and coupled back into the single-mode fiber. Due to a y-coupler in the optical fiber path, the interference signal is led to a photodiode, where the intensity of the optical signal is converted into an electrical current. This electrical signal is then converted into a voltage, filtered by an analogue filter, amplified, and afterward digitized by an analog-to-digital converter in order to finally process the signal in real-time using an field programmable gate array. Compared to the previous version of the ICDS (shown in [20]), the sensor presented in this work is significantly reduced in its geometrical dimensions. The size was reduced from approx. $40 \times 40 \times 48\,\mathrm{mm}^3$ (width, height, depth) to $12 \times 25 \times 17.5\,\mathrm{mm}^3$. The miniaturized ICDS uses a different ultrasonic transducer in favor of reduced geometric dimensions in order to axially deflect the reference mirror. This results in a maximum data rate of 80 kHz compared to 116 kHz of the previous ICDS. Since no special optomechanical component is needed and most components are commercially available, the production costs of the ICDS are relatively low. Furthermore, the sensor housing can be made by additive manufacturing, e.g. by selective laser sintering. A photograph of the miniaturized ICDS is depicted in figure 1(b).

Due to the actuated reference mirror, the interferometer arms can be balanced without an additional increase in the geometrical dimensions. Therefore, a wavelength drift during the measurement process hardly changes the measured height value [20]. A further advantage of the miniaturized ICDS compared to the previous one is an increased signal quality caused by aspherical focusing lenses in both, the measurement and the reference arm. A more detailed comparison between these sensors is given in [22]. In case of the miniaturized ICDS the effective numerical aperture (NA) of the aspherical lens in the measurement arm is approx. 0.21, as shown in [23]. Assuming a Gaussian beam the lateral resolution can be expressed by the minimum beam waist radius [24]

$$w_0 = \frac{\lambda}{\pi \arcsin(\mathrm{NA})} \tag{1}$$

with the wavelength λ of the laser light. Since the end-face of the single-mode fiber acts as a pinhole due to a core diameter of 5 µm, a confocal effect occurs, which leads to a reduced minimum waist radius of approx. $w_{0c} = 0.75 w_0$ according to investigations in [23, 25].

In the case of a depth scan, where the distance between the sensor and the surface under investigation is continuously changed while the interference is captured by the photodiode in equidistant time steps, the side lobes of the acquired depth response signal are strongly reduced in their intensities, as a consequence of the confocal effect. In contrast, axial

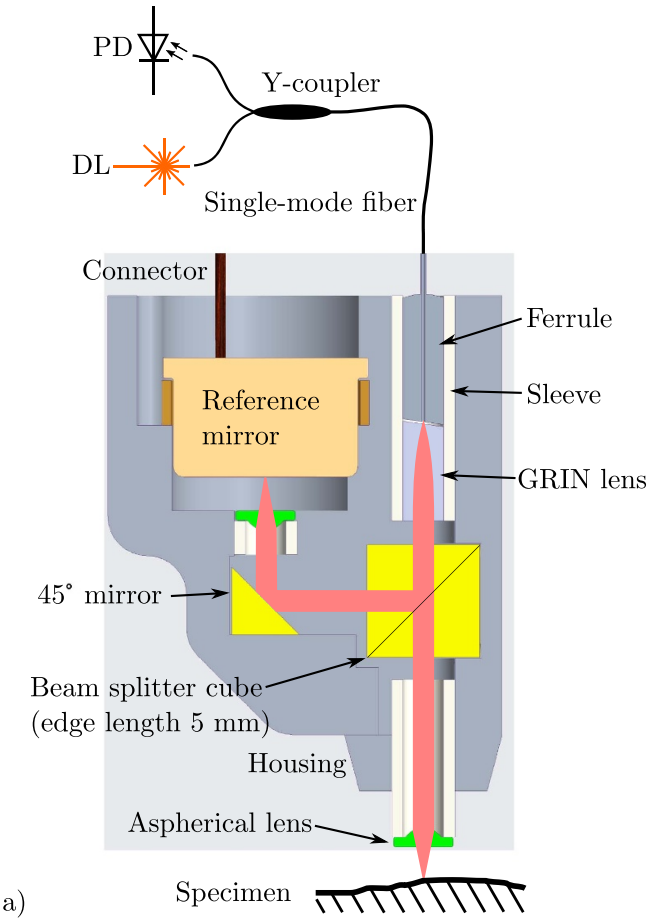

Figure 1. (a) Schematic illustration and (b) photograph of the corresponding ICDS. PD represents the photodiode and DL the diode laser.

filtering of the depth response signals by the confocal effect slightly affects the main lobe as reported in first investigations by Siebert *et al* [23]. Note that this effect is hardly relevant for signal processing carried out in the following section since no depth scan is required for height determination. The resulting displacement range is defined by the depth of field corresponding to twice the Rayleigh length of the focused laser beam, which is approx. 30 µm for the presented sensor setup. Even at higher axial displacements height information is obtained by the sensor without changing the sensor setup. However, the lateral resolution deteriorates with increasing displacement range. The working distance of the ICDS with respect to the surface under investigation is approx. 0.8 mm.

2.2. Signal processing

The collected intensity signal can be expressed by the two-beam interference equation

$$I(x,y) = I_{\mathrm{m}}(x,y) + I_{\mathrm{r}} + 2\sqrt{I_{\mathrm{m}}(x,y)I_{\mathrm{r}}}\cos\left(\phi(x,y)\right) \qquad (2)$$

with $I_{\mathrm{m}}(x,y)$ and I_{r} representing the intensity of the measurement and reference arm obtained from a certain point of the corresponding surface specified by the coordinates (x,y). Note that the polished surface of an ultrasonic transducer acts as reference mirror. This enables a sinusoidal modulation of the OPD by a periodic deflection of the transducer surface in axial direction. As a consequence, the phase

$$\phi(x,y) = \frac{4\pi}{\lambda}\left[z_{\mathrm{a}}\cos\left(2\pi f_{\mathrm{a}}t\right) - \Delta z_{\mathrm{m}}(x,y)\right] \qquad (3)$$

undergoes a modulation with the amplitude z_{a} and the frequency f_{a} of the oscillating reference mirror. In addition, a height change of the measurement surface leads to the alteration $\Delta z_{\mathrm{m}}(x,y)$ of the OPD and thus a corresponding phase shift. The resulting interference signal is depicted in figure 2. Assuming a linear deflection at the flank of the sinusoidal reference mirror movement (visualized by the red dashed line), the fringe frequency f_{e} of the interference signal in the range of the approximately linear deflection over time can be expected as constant. These signal sections are used for phase determination. Due to the linear relation, equation (3) can be simplified by

$$\phi(x,y) \approx \frac{4\pi}{\lambda}\left(z_{\mathrm{a}}2\pi f_{\mathrm{a}}(\pm t - m f_{\mathrm{a}}^{-1}) - \Delta z_{\mathrm{m}}(x,y)\right) \qquad (4)$$

for the signal sections covered by the evaluation windows, where m describes the temporal location of each window. With $f_{\mathrm{e}} = 4\pi f_{\mathrm{a}} z_{\mathrm{a}} \lambda^{-1}$, the phase $\phi(x,y)$ of the interference signal with respect to each evaluation window is calculated using the lock-in technique [26, 27]:

$$\phi(x,y) = \arg\left(\sum_{n=0}^{N_{\mathrm{w}}-1} I(x,y,n)W(n)\exp\left(-\mathrm{i}2\pi n\frac{f_{\mathrm{e}}}{f_{\mathrm{s}}}\right)\right). \qquad (5)$$

Here, f_{s} represents the sampling rate of 50 MHz and n is the index of a sample point in the evaluation window comprising N_{W} sample points in total. To reduce effects caused by the leakage effect the intensity values $I(x,y,n)$ are multiplied by a window function $W(n)$. Due to the arctan2-function, the calculated phase values are limited to the range from $-\pi$ to π.

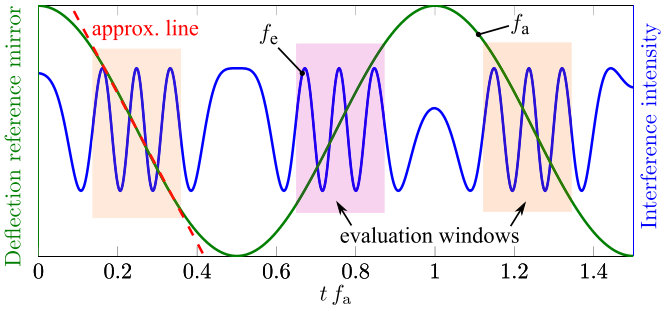

Figure 2. Interference signal (blue) resulting from the sinusoidal deflection of the oscillating reference mirror (green).

Phase values outside this range are wrapped, i.e. phase jumps of $\pm\pi$ between two consecutive phase values occur. In order to remove such phase jumps, a phase unwrapping algorithm is used, i.e. all phase values following the phase jump are corrected by an offset of 2π or -2π. The phase limitation of arctan2 leads to an unambiguous range of $\pm 0.25\lambda$ between two consecutive height values.

Assuming constant frequency f_a and deflection amplitude z_a of the oscillating reference mirror, the difference between consecutively calculated phase values $\Delta\phi(x,y)$ results in the relative height value

$$h(x,y) = \frac{\lambda}{4\pi}\Delta\phi(x,y). \tag{6}$$

However, only phase values belonging to the same flank of the reference mirror deflection, i.e. falling or rising flank, may be subtracted from each other. The calculated height values obtained from the different flanks can finally be combined, leading to a maximum acquisition rate of $2f_\mathrm{a}$ height values per second. This means that for an ultrasonic transducer oscillating at 40 kHz, 80.000 height values per second are obtained using both flanks for evaluation and a rate of 40.000 height values per second in case of a single flank.

3. Results

In order to show the ability to measure specular and rough surfaces using the ICDS, measurement results obtained from different surfaces are studied. Besides two roughness standards specified by different degree of roughness, a sinusoidal standard is additionally measured. Note that a height value rate of 40 kHz and a laser with a wavelength of 1490 nm is used as light source in the ICDS for the following measurements. An advantage of using infrared light is the higher unambiguous range compared to lower wavelengths. In addition, wavelengths between 1300 nm and 1550 nm are used in optical communication systems, which means that there is a more diverse product range of low-price high-quality optical components. Note that the deflection amplitude z_a of the oscillating reference mirror used for the measurements conducted throughout this paper is approx. 1.5 µm. This value can vary dependent on the used control voltage and oscillation frequency.

The axial positioning of the ICDS with respect to the object under investigation is performed by a linear stage mounted on a granite portal. Furthermore, the lateral scan is performed by moving the object under investigation using air-bearing positioning axes. Vibrations emitted by these axes are investigated in [22].

3.1. Roughness standards

An important characteristic to describe the surface irregularity of an object is given by a certain roughness value. These are often defined by the parameters R_a, R_z and R_max. For this purpose, the measured profile is filtered to separate the roughness from the waviness and shape, applying the spatial cutoff filter with a filter wavelength Λ_c, which depends on the expected roughness values R_a and R_z as specified in DIN EN ISO 4288 [28]. In this work, the filtering is achieved using a Gaussian low-pass filter according to DIN EN ISO 16610-21 [29] applied to a measured profile h with a lateral extension of $L_\mathrm{n} = 5\Lambda_\mathrm{c}$. Then, the arithmetic mean R_a, the mean height R_z and the maximum height R_max are calculated according DIN EN ISO 4287 [30].

In the following, roughness parameters are obtained for five profiles laterally shifted in orthogonal direction compared to the direction of the respective measured profile. The relative deviation from the nominal value is defined by

$$\epsilon_{R_a} = \frac{R_a - R_{a,\mathrm{nom}}}{R_{a,\mathrm{nom}}} \tag{7}$$

for the arithmetic mean roughness and analogously for the other parameters. The roughness of a surface is typically measured by a tactile stylus instrument. Therefore, the tactile stylus instrument GD26 with the stylus BFW 10-45-2/90° from Mahr GmbH is used for comparison with the measurement results using the ICDS. Furthermore, identical processes for filtering and determination of roughness parameters are applied to the height profiles acquired by GD26 and ICDS. Both, the tactile instrument and the ICDS are calibrated by repeated measurements on a groove depth standard comprising several groove depths, as shown in [22].

First, surface profiles are obtained from the superfine roughness standard KNT 4070/03 manufactured by Halle GmbH [31, 32] and compared in figure 3. In case of the profile (blue) obtained by the GD26 the used lateral scan velocity was 0.5 mm s^{-1}, whereas three different profiles sampled with 1 mm s^{-1} (black), 20 mm s^{-1} (red) and 75 mm s^{-1} (orange) are exemplary depicted for the ICDS. As shown, the profiles obtained by the ICDS look very similar compared to that of the GD26. With increasing scan velocity a low-pass filtering effect occurs, what can be seen by comparing the profiles obtained with 1 mm s^{-1} and 75 mm s^{-1}. In table 1, the calculated roughness parameters and the corresponding relative deviations according to the previously described procedure are listed. Note that the nominal roughness parameters of the standard are $R_a = 25.2$ nm, $R_z = 136$ nm and $R_\mathrm{max} = 181.1$ nm according to the manufacturer's measurement results obtained with the tactile instrument GD25 from Mahr GmbH. As shown

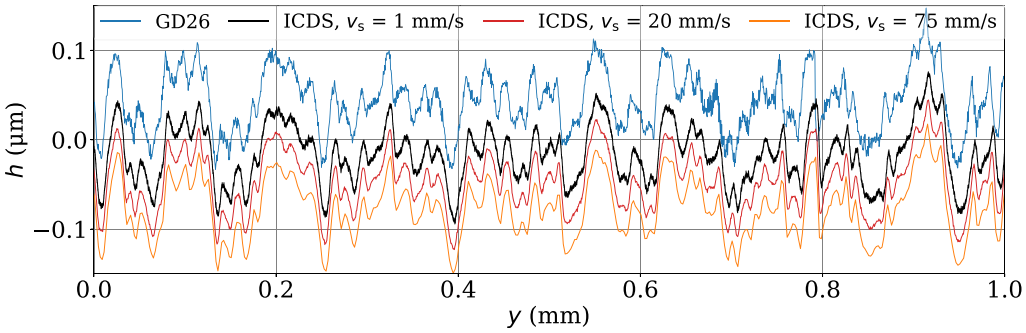

Figure 3. Comparison of profiles obtained from a superfine roughness standard using the tactile stylus instrument GD26 and the optical profilometer ICDS.

Table 1. Roughness parameters of the superfine roughness standard KNT 4070/03 obtained for lateral scanning velocities v_s.

Sensor	v_s (mm s^{-1})	R_a (nm)	ϵ_{R_a} (%)	R_z (nm)	ϵ_{R_z} (%)	R_{max} (nm)	$\epsilon_{R_{max}}$ (%)
GD26	0.5	27.3	8.3	155.3	14.2	201.4	11.2
ICDS	1	26.2	4.0	143.9	5.8	185.6	2.4
	20	26.3	4.4	140.2	3.1	165.6	−8.7
	50	26.1	3.6	136.7	0.5	164.6	−9.2
	75	26.2	4.0	138.1	1.5	165.3	−8.8

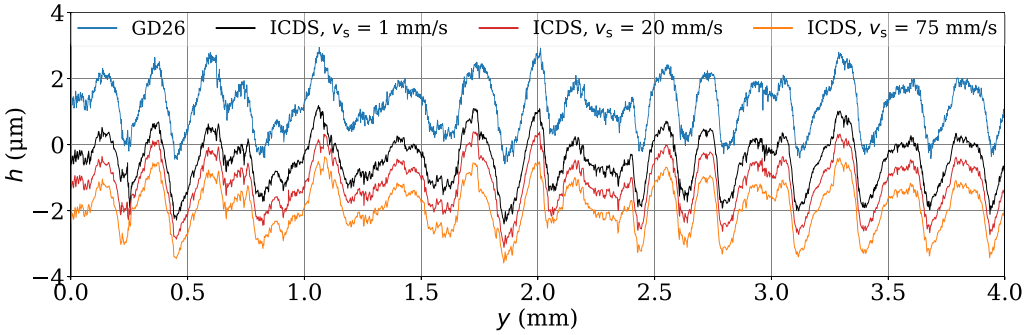

Figure 4. Comparison of profiles obtained from the roughness standard KNT 4058/03 using the tactile stylus instrument GD26 and the optical profilometer ICDS.

in table 1, the R_a values obtained by the ICDS for various scan velocities are nearly the same with a relative deviation of approx. 4% from the nominal value. The determined R_z values show also low relative deviations from the nominal values, whereas those of the R_{max} values increase to approx. 9% for the higher scan velocities of 20 mm s^{-1}. These results might be a consequence of the low-pass filtering effect due to increasing scan velocities. Note that the lateral sampling intervals are below or equal to 0.5 µm for scan velocities up to 20 mm s^{-1} and thus the resulting roughness parameters are determined in accordance with DIN EN ISO 3274 [33]. In case of the profile obtained at a lateral scan velocity of 75 mm s^{-1}, a lateral sampling interval of approx. 1.8 µm occurs, which is higher than the value recommended by DIN EN ISO 3274. This sampling interval can still be reduced below 1 µm using both signal flanks for evaluation, resulting in a data rate of 80 kHz.

The roughness parameters obtained by the tactile stylus instrument show higher values and thus higher deviations up to 20.3 nm for R_{max} measured by GD26 compared to the nominal value of $R_{max} = 181.1$ µm given by the manufacturer. The tactile stylus instrument is characterized by a residual uncertainty value of $R_z \leqslant 50$ nm for a lateral scan velocity of 0.5 mm s^{-1} as specified by the manufacturer according to DIN EN ISO 3274 [33]. In contrast, the ICDS shows a standard deviation of approx. 1 nm for repeated measurements at the same position of a mirror under investigation, as discussed in [22].

As second measurement object, the roughness standard KNT 4058/03 grade 2 from Halle GmbH [34] is used. The profiles measured by GD26 and ICDS are depicted in figure 4. Except from deviations caused by phase jumps in the profiles measured by the ICDS (see profiles at the lateral position $y = 1.7$ µm), these profiles are also in good agreement. Note that the phase jumps are not corrected for calculating the roughness parameters of the roughness standards. A reason for further small deviations is due to different lateral locations on the surface under investigation. Despite different scan velocities for the profiles obtained by the ICDS, deviations caused by low-pass filtering are hardly observable in these profiles. However, some phase jumps can be observed in the profiles

Table 2. Roughness parameters of the roughness standard KNT 4058/03 grade 2 obtained for lateral scanning velocities v_s.

Sensor	v_s (mm s^{-1})	R_a (nm)	ϵ_{R_a} (%)	R_z (nm)	ϵ_{R_z} (%)	R_{max} (nm)	$\epsilon_{R_{max}}$ (%)
GD26	0.5	643.5	2.5	3114.3	3.8	3510.3	3.5
ICDS	1	614.7	−2.1	3070.8	2.4	3386.8	0.8
	20	637.5	1.5	3074.6	2.5	3320.9	−1.2
	50	617.4	−1.7	2878.3	−4.1	3181.4	−5.3
	75	606.3	−3.5	2896.5	−3.5	3146.2	−6.4

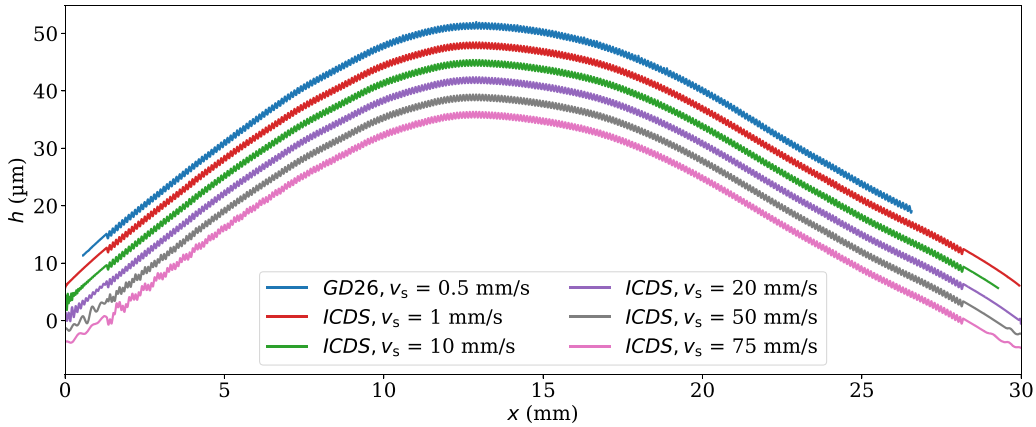

Figure 5. Profile of the sinus standard 531 measured by GD26 and ICDS with various lateral scan velocities.

at approx. $y = 0.2$ mm and $y = 1.1$ mm. The nominal roughness values $R_a = 0.628$ µm, $R_z = 3$µm and $R_{max} = 3.36$µm of the roughness standard are specified by calibration measurements from the manufacturer using the tactile stylus instrument GD25 from Mahr GmbH. These values are characterized by a relative measurement uncertainty of ±7%. The roughness parameters obtained by the IDCS and the GD26 are listed in table 2. As shown, the relative deviations from the nominal values are low and below the given uncertainty of ±7%. With increasing lateral scan velocity the deviations increase slightly for the ICDS, especially for the R_{max} value. Overall, these measurement results show that roughness is measurable with the ICDS even at high lateral scan velocities up to 75 mm s^{-1}.

3.2. Sinusoidal standard

In addition, measurement results obtained from a sinusoidal surface are compared. For this purpose the sinusoidal standard 531 from Rubert & Co. Ltd [35] comprising a peak-to-valley (PV) amplitude of 1 µm and a period length of 100 µm is used. Again, multiple measurements are performed with the ICDS using different scan velocities v_s compared to a reference measurement performed by the tactile stylus instrument GD26. Besides the sinusoidal structure the measurement surface exhibits an additional shape as shown by multiple profiles measured along the entire surface depicted in figure 5. Since the maximum lateral scan range of the GD26 is limited by 26 mm, a profile comprising the entire structure could not be measured with this instrument. In case of the ICDS one of the lateral positioning axes of a multisensor measuring sensor [25, 36] is used for the lateral scan. The positioning range covers the length of the profile to be measured and thus, a profile comprising the entire surface structure could be measured by the ICDS. The profile section obtained by the GD26 shows a similar shape compared to profiles measured by the ICDS. Low deviations might be a result of slightly different measurement positions on the specimen. In contrast, the shapes of the profiles obtained by the ICDS are identical. The main differences between the shown profiles are due to oscillations, which result from vertical vibrations caused by the acceleration of the scan axis and become stronger, if the scan velocity is increased. With regard to the measurement results obtained by ICDS, the height difference between the maximum and the height from where the sinusoidal structure starts or ends corresponds to approx. 36 µm. The sinusoidal structure extends over a lateral length of approx. 27 mm.

A section of the measured profiles is depicted in figure 6. Note that the height differences between the profiles are reduced to increase comparability. Both, the GD26 profile and the ICDS profiles for different scan velocities show the sinusoidal structure with a period length of approx. 100 µm. In case of the profile obtained by the tactile stylus instrument small deviations from the perfect sinusoidal shape are observable, which result from contamination of the specimen. Furthermore, a high-frequency roughness is superimposed to the sinusoidal structure. Its origin can be attributed to milling traces of the negative mold during manufacturing and are less pronounced in case of the profiles obtained by the ICDS. This is probably a consequence of the limited lateral resolution and an additional filtering of the measured profile due to the different lateral scan velocities, which lead to an extension of the relevant filtering width according to equation (1) [20]:

$$w_F = 2w_0 + \frac{v_s}{2f_a} w_e, \tag{8}$$

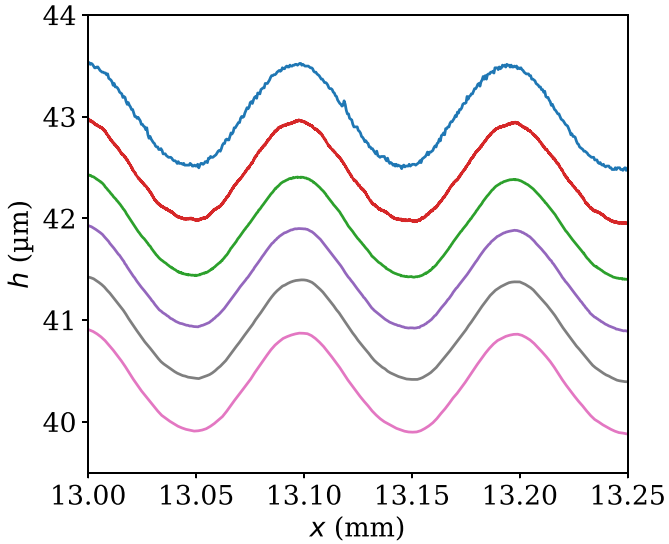

Figure 6. section of the sinusoidal profiles from figure 5 with reduced vertical offsets for better comparability. For legend see figure 5.

Table 3. PV-amplitudes h_{pv} obtained from the sinusoidal profiles depicted in figure 6 for various lateral scanning velocities v_s.

Sensor	v_s (mm s^{-1})	h_{pv} (nm)
GD26	0.5	986.9
ICDS	1	986.8
	10	986.8
	20	985.1
	50	986.8
	75	984.8

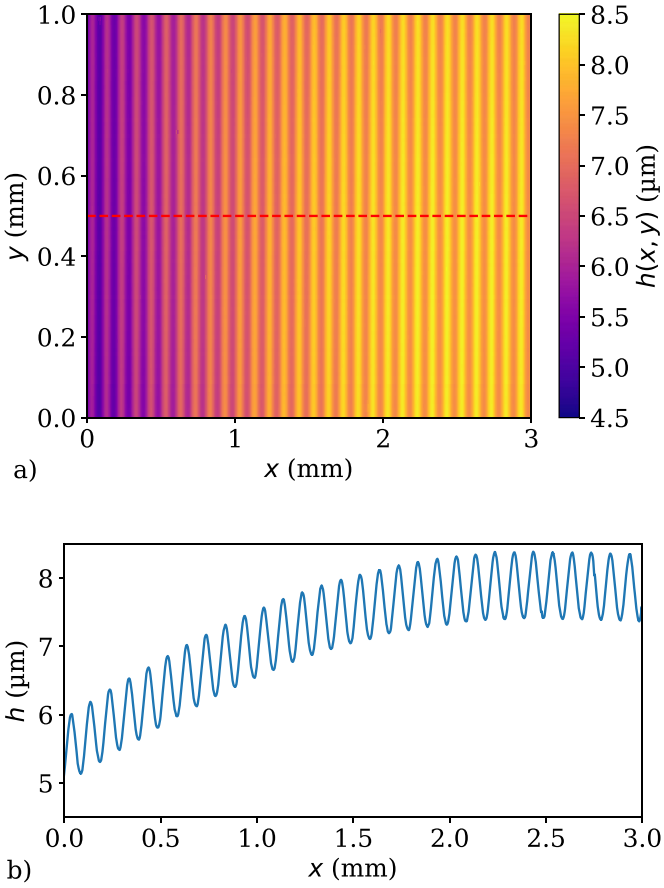

Figure 7. (a) Sinusoidal surface topography measured by the ICDS with a lateral scan velocity of 10 mm s^{-1} and (b) a profile extracted from the red dashed line in (a).

where w_e represents the fraction of a half period $(2f_a)^{-1}$. This means that with increasing scan velocity, the filtering affects the measured profile stronger. The filtering width can be reduced by an increased data rate using an increased actor frequency f_a or a lower w_e as well as a higher NA of the sensor tip. However, a reduced w_e leads to a lower ratio of fringes for evaluation (see figure 2) and thus decreases the axial accuracy of the sensor.

In order to determine the PV-amplitudes of the presented profiles, several individual PV-amplitudes are taken from the corresponding profile of the section shown in figure 6. Their averages are calculated and listed in table 3 for comparison. Based on these values it can be assumed that the real PV-amplitude is slightly below the nominal value of 1 µm, what is in agreement with previous studies [22].

Besides single profiles, full-field measurements of surface topographies under investigation are also possible with the ICDS. This is demonstrated in figure 7 for the sinusoidal grating 531 used before. Multiple profile measurements are conducted by the ICDS, while the specimen is laterally shifted in orthogonal direction to the scanning trace. In case of the shown surface topography a lateral shift of $\Delta y = 10$ µm is used. Tracking the lateral positioning values using a quadrature encoder of the scan axes, each measured height value is assigned to a lateral position in real time. This enables the lateral combination of multiple individual profiles, resulting in 1.2 million height values for the measured surface topography. The full-field measurement of surface topography allows the application of a 2D-unwrapping algorithm as described by Herráez *et al* [37], leading to a robust correction of potential phase jumps.

4. Conclusions

We present a new ICDS device with minimized geometric dimensions and improved signal quality compared to the previous sensor design [20]. Due to the smaller geometric dimensions, the sensor can be more easily integrated into existing measurement systems and, in addition, an improved accessibility of difficult to access surfaces is given. The sensor head comprising an aspherical focusing lens can be changed depending on the application, e.g. by introducing a prism in front of the sensor head in order to achieve a 90° deflection of the focused beam similar to the solutions presented in [3, 16].

The ICDS is able to measure specularly reflecting as well as rough surfaces and thus enables the determination of roughness parameters even for higher roughness values. Furthermore, the investigated surfaces could be measured at high

lateral scan velocities up to 75 mm s^{-1}. This constitutes short measurement times and is thus a benefit compared to profilometers such as tactile stylus instruments. Higher lateral scan velocities are also possible using the ICDS but lead to a decreased lateral resolution [36]. Note that the acquisition rate of height values depends on the oscillation frequency of the ultrasonic transducer acting as reference mirror. Therefore, the data rate can be further increased using a higher oscillation frequency and thus a better lateral resolution can be achieved at higher scan velocities. Likewise, the NA of the sensor head can be increased by changing the focusing lens to improve the lateral resolution and the ability to measure higher slope angles depending on the field of application. The correct choice of the scan velocity is also important for full-field measurements using the ICDS, since vertical oscillations depending on the speed of the scan axis affect the measured profile. In case of small measurement fields, it might be appropriate to use a low scan velocity, e.g. 10 mm s^{-1} in the given example. Then, consecutive height values can be averaged to improve the axial measuring uncertainty of the sensor. In addition, the localization of possible vibration sources and the reduction of their influence on measured height values are part of further investigations to improve the axial accuracy of the sensor. Overall, the ICDS is a relatively low-cost profilometer for precise high-speed measurements of surface texture in the micro- and nanometer range.

Data availability statement

The data that support the findings of this study are available upon reasonable request from the authors.

Acknowledgments

The authors gratefully acknowledge the financial support of the research project: Zentrales Innovationsprogramm Mittelstand (ZIM) Project ZF4126411DF8 founded by the Federal Ministry for Economic Affairs and Energy of Germany.

ORCID iDs

Sebastian Hagemeier https://orcid.org/0000-0002-3057-0034
Peter Lehmann https://orcid.org/0000-0003-0051-5066

References

[1] Conerty M D, Castracane J, Saravia E, Parnes S M and Cacace A T 1992 Development of an otolaryngological interferometric fiber optic diagnostic probe *Proc. SPIE* **1649** 98–105
[2] Lehmann P, Lücke P, Mohr J, Moran-Iglesias C J, Osten W, Ruprecht A and Schönfelder S 2009 Optical measuring head *US Patent* US 7,486,394 B2
[3] Pfeifer T, Schmitt R, Konig N and Mallmann G F 2011 Interferometric measurement of injection nozzles using ultra-small fiber-optical probes *Chin. Opt. Lett.* **9** 071202
[4] Messerschmidt B 2015 Corrective fiber-optic microprobe for white light interferometric measurements *US Patent* 9,074,862
[5] Jiang X, Wang K and Martin H 2006 Near common-path optical fiber interferometer for potentially fast on-line microscale-nanoscale surface measurement *Opt. Lett.* **31** 3603–5
[6] Gronle M, Lyda W, Mauch F and Osten W 2011 Laterally chromatically dispersed, spectrally encoded interferometer *Appl. Opt.* **50** 4574–80
[7] Molesini G, Pedrini G, Poggi P and Quercioli F 1984 Focus-wavelength encoded optical profilometer *Opt. Commun.* **49** 229–33
[8] Browne M, Akinyemi O and Boyde A 1992 Confocal surface profiling utilizing chromatic aberration *Scanning* **14** 145–53
[9] Ruprecht A, Wiesendanger T and Tiziani H 2004 Chromatic confocal microscopy with a finite pinhole size *Opt. Lett.* **29** 2130–2
[10] Dobson S L, Sun P-C and Fainman Y 1997 Diffractive lenses for chromatic confocal imaging *Appl. Opt.* **36** 4744–8
[11] Garzón J, Meneses J, Tribillon G, Gharbi T and Plata A 2004 Chromatic confocal microscopy by means of continuum light generated through a standard single-mode fibre *J. Opt. A: Pure Appl. Opt.* **6** 544
[12] Mastylo R, Dontsov D, Manske E and Jager G 2005 A focus sensor for an application in a nanopositioning and nanomeasuring machine *Proc. SPIE* **5856** 238–44
[13] Rao Y-J and Jackson D A 1996 Recent progress in fibre optic low-coherence interferometry *Meas. Sci. Technol.* **7** 981
[14] Depiereux F, Lehmann P, Pfeifer T and Schmitt R 2007 Fiber-optical sensor with miniaturized probe head and nanometer accuracy based on spatially modulated low-coherence interferogram analysis *Appl. Opt.* **46** 3425–31
[15] Beutler A 2016 Flexible, non-contact and high-precision measurements of optical components *Surf. Topography: Metrol. Prop.* **4** 024011
[16] Schulz M and Lehmann P 2013 Measurement of distance changes using a fibre-coupled common-path interferometer with mechanical path length modulation *Meas. Sci. Technol.* **24** 065202
[17] Schake M, Schulz M and Lehmann P 2015 High-resolution fiber-coupled interferometric point sensor for micro- and nano-metrology *tm-Tech. Mess.* **82** 367–76
[18] Sharma S, Eiswirt P and Petter J 2018 Electro optic sensor for high precision absolute distance measurement using multiwavelength interferometry *Opt. Express* **26** 3443–51
[19] Sharma S, Eiswirt P and Petter J 2019 Multi-wavelength interferometric distance sensors *Advances in Optics: Reviews* vol 4 ed Y Y Sergey (Barcelona: IFSA Publishing, S.L.) ch 10, pp 239–64
[20] Hagemeier S, Tereschenko S and Lehmann P 2019 High-speed laser interferometric distance sensor with reference mirror oscillating at ultrasonic frequencies *tm-Tech. Mess.* **86** 164–74
[21] Malacara D 2007 *Optical Shop Testing* vol 59 (New York: Wiley)
[22] Hagemeier S 2022 Comparison and investigation of various topography sensors using a multisensor measuring system *PhD Thesis* University of Kassel, Germany (https://doi.org/10.17170/kobra-202208186691)
[23] Siebert M, Hagemeier S, Pahl T, Serbes H and Lehmann P 2022 Modeling of fiber-coupled confocal and interferometric confocal distance sensors *Meas. Sci. Technol.* **33** 075104
[24] Kogelnik H and Li T 1966 Laser beams and resonators *Appl. Opt.* **5** 1550–67

[25] Hagemeier S, Schake M and Lehmann P 2019 Sensor characterization by comparative measurements using a multi-sensor measuring system *J. Sens. Sens. Syst.* **8** 111–21
[26] Meade M 1982 Advances in lock-in amplifiers *J. Phys. E: Sci. Instrum.* **15** 395–403
[27] Masciotti J M, Lasker J M and Hielscher A H 2007 Digital lock-in detection for discriminating multiple modulation frequencies with high accuracy and computational efficiency *IEEE Trans. Instrum. Meas.* **57** 182–9
[28] DIN EN ISO 4288 2010 *Geometrical Product Specification (GPS)—Surface Texture: Profile Method—Rules and Procedures for the Assessment of Surface Texture* (International Organisation for Standardization)
[29] DIN EN ISO 16610-21 2013 *Geometrical Product Specification (GPS)—Filteration—Part21: Linear Profile Filters: Gaussian Filters* (International Organisation for Standardization)
[30] DIN EN ISO 4287 2010 *Geometrical Product Specification (GPS)—Surface Texture: Profile Method—Terms, Definitions and Surface Texture Parameters* (International Organisation for Standardization)
[31] Halle GmbH 2009 Calibration standards for contact stylus instruments, line of products KNT 4070/03 (requested in 2022) (available at: www.halle-normale.de/pdf/Prospektseiten/englisch/17%20Ps-KNT4070_03_Bl_6-6_GB.pdf)
[32] Halle GmbH 2009 KNT 4070/03—Nominal values of the ultra fine roughness measurement standards (requested in 2022) (available at: www.halle-normale.de/pdf/Prospektseiten/englisch/16%20Ps-KNT-4070_Bl_6-2_GB.pdf)
[33] DIN EN ISO 3274 1996 *Geometrical Product Specification (GPS)—Surface Texture: Profile Method—Nominal Characteristics of Contact (Stylus) Instruments* (International Organisation for Standardization)
[34] Halle GmbH 2009 Roughness measurement standards—line of products KNT 4058/03 (requested in 2022) (available at: www.halle-normale.de/pdf/Prospektseiten/englisch/10%20Ps-KNT-4058_03_Bl_3-1_GB.pdf)
[35] Rubert & Co Ltd Reference specimens (requested in 2022) (available at: www.rubert.co.uk/reference-specimens/)
[36] Hagemeier S and Lehmann P 2018 Multisensorisches messsystem zur untersuchung der übertragungseigen schaften von topographiesensoren *tm-Tech. Mess.* **85** 380–94
[37] Herráez M A, Burton D R, Lalor M J and Gdeisat M A 2002 Fast two-dimensional phase-unwrapping algorithm based on sorting by reliability following a noncontinuous path *Appl. Opt.* **41** 7437–44